Journal of
Synchrotron
Radiation

ISSN 0909-0495

Received 27 March 2011
Accepted 2 August 2011

Synchrotron X-ray tests of an L-shaped laterally graded multilayer mirror for the analyzer system of the ultra-high-resolution IXS spectrometer at NSLS-II

Marcelo G. Honnicke,[a]‡ Jeffrey W. Keister,[a] Raymond Conley,[a] Konstantine Kaznatcheev,[a] Peter Z. Takacs,[b] David Scott Coburn,[a] Leo Reffi[a] and Yong Q. Cai[a]*

[a]National Synchrotron Light Source II, Brookhaven National Laboratory, USA, and [b]Instrumentation Division, Brookhaven National Laboratory, USA. E-mail: cai@bnl.gov

Characterization and testing of an L-shaped laterally graded multilayer mirror are presented. This mirror is designed as a two-dimensional collimating optics for the analyzer system of the ultra-high-resolution inelastic X-ray scattering (IXS) spectrometer at National Synchrotron Light Source II (NSLS-II). The characterization includes point-to-point reflectivity measurements, lattice parameter determination and mirror metrology (figure, slope error and roughness). The synchrotron X-ray test of the mirror was carried out reversely as a focusing device. The results show that the L-shaped laterally graded multilayer mirror is suitable to be used, with high efficiency, for the analyzer system of the IXS spectrometer at NSLS-II.

Keywords: X-ray optics; X-ray mirrors; L-shaped mirror; nested mirror; Montel optics; Kirkpatrick–Baez geometry.

1. Introduction

Diffractive multilayer mirrors have been widely used in X-ray optics. One distinctive advantage compared with reflective mirrors is that the angle of incidence can be substantially increased, providing a much larger angular acceptance with shorter mirror length and less stringent slope error requirements. In the X-ray spectral range, multilayer mirrors were first successfully fabricated in the early 1940s as superlattices using evaporation techniques (DuMond & Youtz, 1940). The multilayer is an artificial structure composed of layers of alternating soft and heavy materials, thereby creating an artificial lattice. Such structures become much more useful (Vinogradov & Zeldovich, 1977; Lienert *et al.*, 1999; Champeaux *et al.*, 2007) with the advent of the new sputtering deposition technique capable of controlling the layer thickness with a precision better than 0.2 nm (Schuster & Gobel, 1995). This makes it possible to build laterally graded multilayers, *i.e.* structures with the lattice parameter (d) varying along the mirror surface. The advantage of such a structure is that the difference in incidence angle along the mirror can be compensated, thereby improving the efficiency of the mirror as a diffractive optics. Laterally graded multilayer mirrors, for example, have been used to increase the bandwidth (to $\Delta\lambda/\lambda \simeq 10^{-3}$) of beamline monochromators. Their use as collimators (Goebel mirrors) in conventional X-ray sources has also been widely employed to improve the intensity in powder diffraction experiments (Hertlein *et al.*, 2005; Shymanovich *et al.*, 2008).

Many applications of multilayer mirrors require two-dimensional figuring. The challenge in fabricating a mirror with an aspherical surface figure can be solved by using L-shaped laterally graded multilayer mirrors which combine two one-dimensionally figured multilayer mirrors mounted 90° to each other (called Montel or nested mirror). Such a kind of mirror has been used in commercial diffractometers (Hertlein *et al.*, 2005; Shymanovich *et al.*, 2008). Reflective L-shaped mirrors have also been tested recently with neutron sources (Ice *et al.*, 2009) and X-ray sources (Liu *et al.*, 2011). By having two diffractions in each surface (Fig. 1*a*), these mirrors can be used to focus (elliptic figure) or collimate (parabolic figure) the beam in two dimensions. They can also be used to focus the beam in one direction and collimate in the other (*e.g.* by combining an elliptic mirror with a parabolic mirror). The disadvantage of having two diffractions, compared with an aspherical mirror where every ray is reflected once, is compensated by the possibility to fabricate a surface with more accurate surface figuring. Furthermore, compared with the Kirkpatrick–Baez geometry (Kirkpatrick & Baez, 1948), L-shaped laterally graded multilayer mirrors present the advantage of having the same focal distance for both the vertical and horizontal mirrors. To simulate such a multilayer

‡ Present address: Universidade Federal de Goias, Campus Jatai, Brazil.

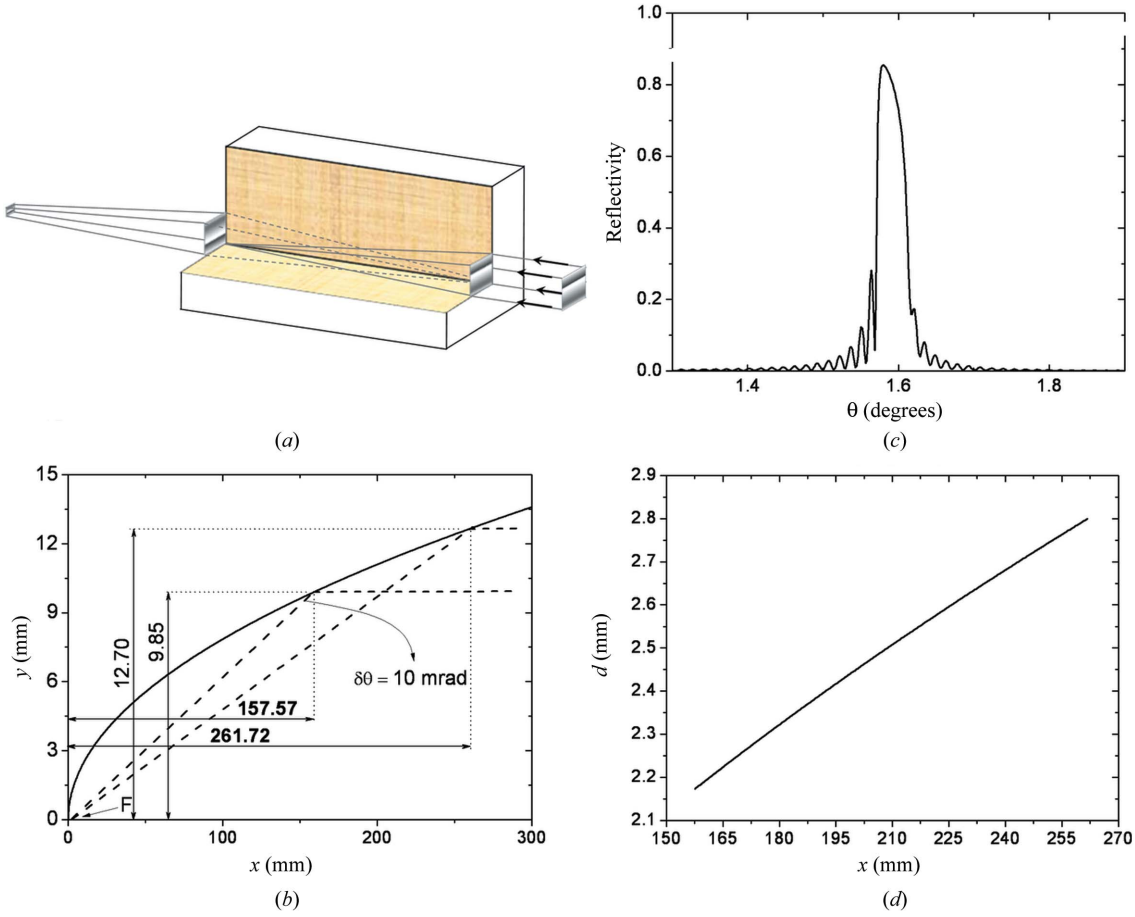

Figure 1
(*a*) Schematic representation of the L-shaped laterally graded multilayer mirror used as a two-dimensional focusing device for an incoming parallel beam (parabolic figure). (*b*) Mirror figure (parabolic) with a parabola parameter, p = 0.308 mm. (*c*) Theoretical reflectivity for a flat Si substrate coated with 100 W/C graded bi-layers (2.5 nm each, W 1.0 nm-thick and C 1.5 nm-thick) at 9.1 keV. (*d*) Lattice parameter, d, *versus* distance along the mirror surface for the parabolic laterally graded multilayer mirror.

mirror, a ray-tracing program, that takes into account both the X-ray refraction and dynamical X-ray diffraction effects (Authier, 2001), has been recently proposed and used for the design of the mirror reported herein (Honnicke *et al.*, 2010).

In this manuscript an L-shaped laterally graded multilayer mirror (Fig. 1*a*) is characterized and tested. The L-shaped laterally graded multilayer mirror was acquired from INCOATEC (Innovative Coating Technologies GmbH). The mirror parameters are chosen to meet the requirements for the analyzer system of the ultra-high-resolution inelastic X-ray scattering (IXS) spectrometer being constructed at National Synchrotron Light Source II (NSLS-II). The L-shaped laterally graded multilayer mirror is designed to collect the scattering from the sample with an angular acceptance of 5 mrad and collimate this beam to 0.1 mrad in both directions for the acceptance of the ultra-high-energy resolution analyzer crystal system (Shvyd'ko *et al.*, 2006; Cai *et al.*, 2009), in order to improve the efficiency of the spectrometer.

Three steps were followed in the characterization and tests: (i) metrology (mirror figure, slope error and roughness); (ii) point-to-point reflectivity of each surface using a conventional X-ray diffractometer; and (iii) mirror test as a two-dimensional optical focusing device in a synchrotron beamline.

2. Mirror parameters

Each element in the L-shaped laterally graded multilayer mirror (Montel optics) is a parabolic cylinder with the same figure and with a graded multilayer coating applied. The dimensions of both surfaces are 120 mm × 20 mm. However, the dimensions of the clear aperture on each surface are ∼100 mm × 18 mm. The angular acceptance is further defined by a fixed aperture to 10 mrad. The theoretical collimation is better than 0.1 mrad for a source size of 5 µm × 5 µm and a source-to-mirror distance (s) of 200 mm. Only the area close to the joint between the two reflecting surfaces is utilized. The parabolic shape is given by the following equations,

$$y = (2px)^{1/2}, \qquad z = (2px)^{1/2}, \tag{1}$$

where p = 0.308 mm is the focal parameter common to both mirrors, which is twice the focal distance ($p = 2F$).

The relation between p, s and the incident angle, θ_i, is given by

$$\theta_i = \operatorname{arccot}\left(\frac{2s}{p} - 1\right). \tag{2}$$

The parabolic figure of the L-shaped mirror, for s = 200 mm and $\theta_i = 1.59^\circ$ (p = 0.308 mm), is shown in Fig. 1(*b*).

The multilayer materials and the number of layers were determined to have the maximum efficiency (acceptance and reflectivity, for a flat multilayer) at 9.1 keV, the operating energy of the ultra-high-energy-resolution analyzer optics (Shvyd'ko *et al.*, 2006; Cai *et al.*, 2009). The L-shaped laterally graded multilayer mirror has a Si substrate coated with 100 W/C graded bi-layers. The theoretical reflectivity for a flat W/C multilayer mirror with 100 bi-layers, with no surface imperfections, is shown in Fig. 1(*c*). The reflectivity curve presents an asymmetry and some oscillations around the main peak. Both effects are a consequence of the dynamical theory of X-ray diffraction (Authier, 2001). The asymmetry is due to the different photoelectric absorption of the standing X-ray wavefield (Honnicke & Cusatis, 2009) for the low- and high-angle side of the rocking curve. The oscillations are the Pendellösung fringes owing to the finite crystal condition. If the multilayers was thicker, *i.e.* the number of bi-layers was larger, these oscillations would disappear. The theoretical values of d along the mirror surface (graded multilayer) are shown in Fig. 1(*d*).

The slope error and roughness on the mirror surfaces required to achieve the specified collimation (0.1 mrad) and efficiency (49%) were 10 µrad RMS and 0.2 nm RMS, respectively. With these parameters a reflectivity of 70% for each surface, or 49% for both surfaces, was expected.

3. Metrology

As mentioned in §1, the required specifications for the L-shaped laterally graded multilayer mirror were chosen in such a way that it could match, with the most possible efficiency, the collimation and beam size requirements for the analyzer crystal system of the ultra-high-resolution IXS spectrometer at NSLS-II. By using our theoretical ray-tracing approach (Honnicke *et al.*, 2010) we found out that to have an angular acceptance of 5 mrad and collimate this beam to 0.1 mrad we should have the following parameters: source-to-mirror distance s = 200 mm, parabola parameter p = 0.308 mm with a slope error and roughness of 10 µrad RMS and 0.2 nm RMS, respectively.

To check whether the acquired mirror was within the specifications, metrology tests (figure, slope error and roughness) were carried out on both surfaces of the L-shaped mirror. Long trace profile (LTP), 4" Fizeau MST VeriFire interferometer and atomic force microscopy (AFM) measurements were made at the Instrumentation Division and at the R&D laboratories of NSLS-II at Brookhaven National Laboratory. A photograph of the L-shaped laterally graded multilayer mirror, specifying the two surfaces, is shown in Fig. 2(*a*).

The LTP measurements were made along the full length of the mirror surface at 5 mm from the junction of the two mirrors (as close as we could go in order to have clearance to measure). Fig. 2(*b*) shows one of the measurements taken on surface 1. Surface 2 has a similar structure, and for this reason is not shown here. A noticeable periodicity in the millimeter range was observed. Excluding the end regions, the computed power spectral density (Fig. 2*c*) shows a spectral period of 4.22 mm and a first harmonic of 2.11 mm. This is most likely the result of the polishing process. However, the RMS slope error is within the specifications (∼8.5 µrad).

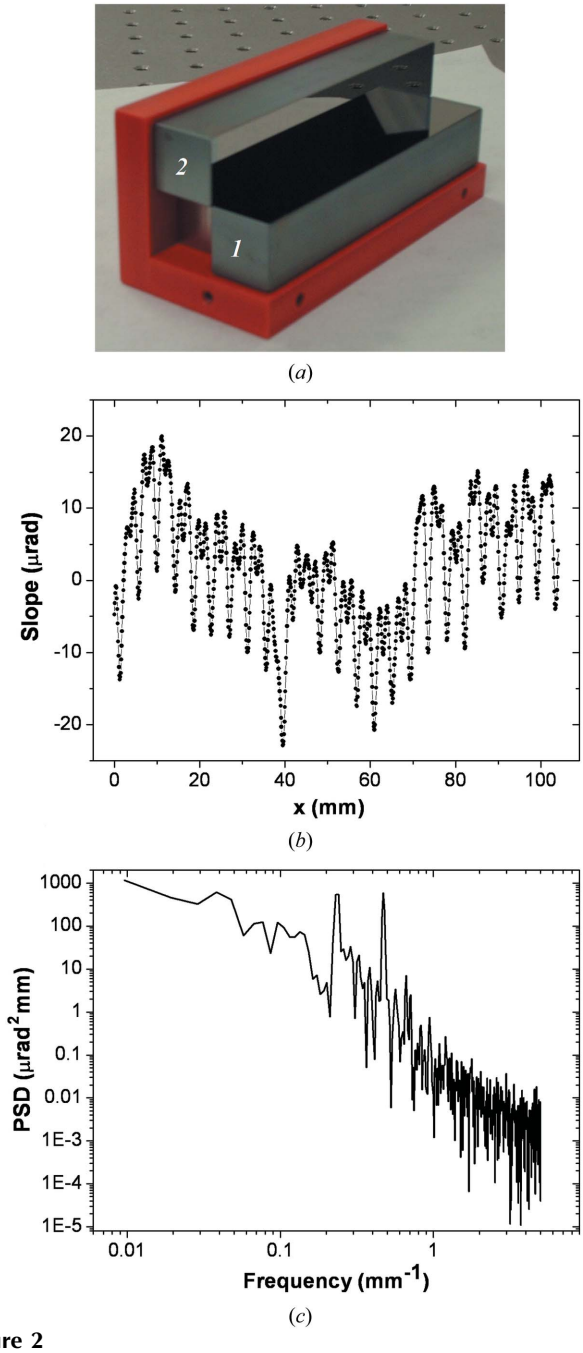

Figure 2
(*a*) L-shaped laterally graded multilayer mirror (Montel optics) showing the two surfaces (1 and 2). (*b*) Long trace profile measurements taken at 5 mm from the junction of the entire length of the L-shaped laterally graded multilayer mirror surface (surface 1). There is a noticeable periodicity in the millimeter range on these surfaces. (*c*) Power spectral density (PSD) (excluding the regions close to the edges), showing that the periodicity has a fundamental frequency of 2.36×10^{-1} mm^{-1} (4.22 mm) and a first harmonic of 4.74×10^{-1} mm^{-1} (2.11 mm). However, the RMS slope error (∼8.5 µrad) is within the specifications.

The Fizeau surface height measurements taken within a 47 mm length of the mirror surface and very close to the corner show a very well defined parabola, with deviations smaller than 25 nm (RMS) (Fig. 3*a*). The slope profiles computed from the Fizeau height measurements result in RMS slope error numbers in the range of 12 µrad (Fig. 3*b*), which are close to the specifications and in general agreement with the LTP measurements. Two-dimensional plots of both mirrors in a 2 mm range from the junction between the two mirrors is shown in Fig. 3(*c*). The trace lengths and detrending are different between Fizeau and LTP measurements, which accounts for the difference. Also, the surface regions were different, being another contributing factor.

The AFM measurements (not shown here) showed roughness below 0.3 nm RMS. This was the level of roughness that could be measured in the NSLS-II R&D laboratories owing to a demolition process that was occurring on-site during these measurements. Therefore, they are expected to be within the specifications, which are 0.2 nm.

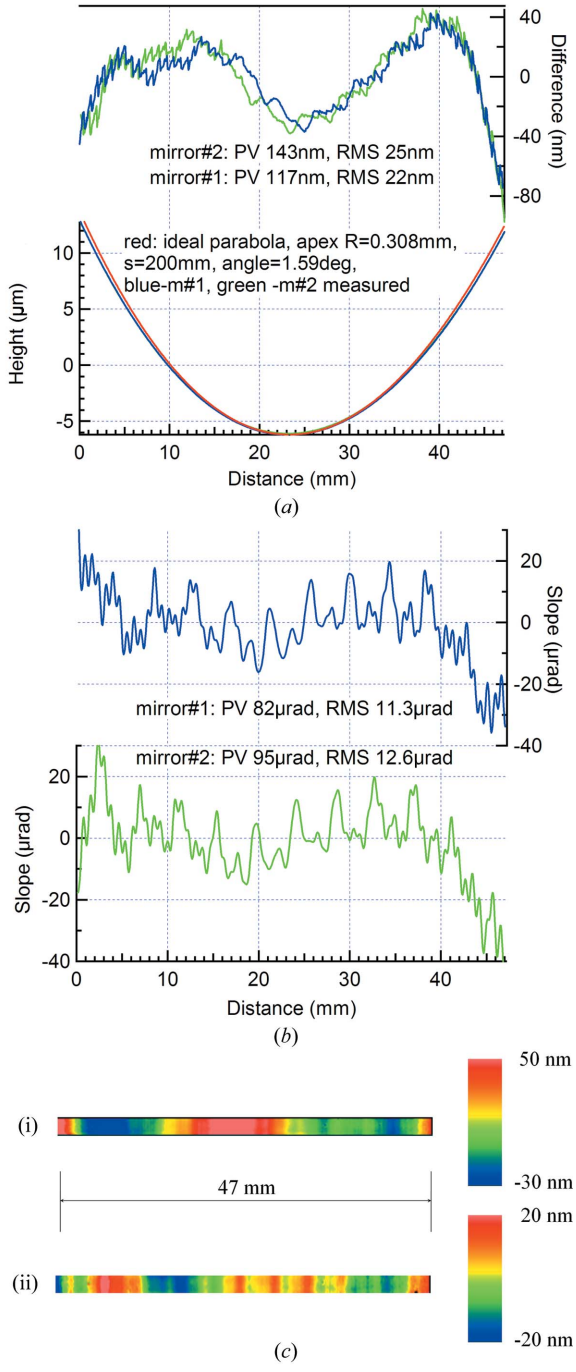

Figure 3
4" Fizeau measurements made at normal incidence to the surface. (*a*) Deviation from the ideal parabola for both surfaces (1 and 2). (*b*) Slope errors (~12 µrad RMS) in a 40 mm distance for both surfaces (1 and 2). The results are consistent with the LTP measurements. (*c*) Two-dimensional plots on the mirror surface in a 2 mm range close to the junction between the two mirrors: (i) surface 1 and (ii) surface 2.

4. Reflectivity measurements

The point-to-point reflectivity measurements on the L-shaped laterally graded multilayer mirror were carried out using a θ–θ X-ray diffractometer at 8.048 keV (Cu $K\alpha_1$), available in the NSLS-II R&D laboratories. The set-up is schematically shown in Fig. 4. All the measurements were taken at each surface independently. A vertical 50 µm slit was used to define the incoming beam on the mirror. Using this, the projected beam footprint on the mirror surface was about 1.6 mm.

The θ–θ geometry does not offer enough flexibility to measure the reflectivity of the entire pre-figured L-shaped mirrors owing to the coupling of the two angles, which makes the zero angle difficult to determine. Measurements were therefore taken only in three points for each surface (two of them close to the edges and the third one in the center). A typical measured reflectivity curve is shown in the inset of

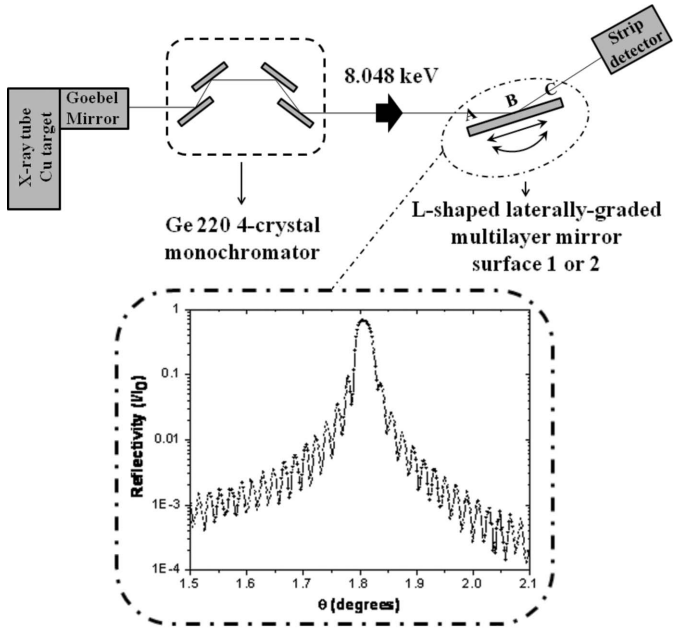

Figure 4
Schematic representation of the reflectivity measurements. A, B and C indicate the positions on both surfaces of the L-shaped laterally graded multilayer mirror where reflectivity measurements were taken. The inset shows the reflectivity curve taken in the position B (center) of surface 1 of the mirror.

Fig. 4. All reflectivity results are shown in Fig. 5(*a*) and compared with the theoretical values. One can see that the reflectivity values (for 8.048 keV) do not agree very well with the theoretical ones. There are several possible causes for this. Firstly, it may be caused by stress in the film, although the measured widths (full width at half-maximum, FWHM) were very close to the theoretical values (590–684 µrad, depending on the mirror surface position with different *d*). Secondly, it could be due to a higher surface roughness than specified; however, the metrology results show that this is within the specifications. Also, interlayer roughness or layer interdiffusion could cause the reflectivity to decrease. However, if this was true the Pendellösung fringes would be much weaker, whereas they were strong in all the measurements. This, joined with consistent measurements presented by INCOATEC previous to our conformance tests, suggests that the reflectivity measurements presented here were not very well optimized owing to the thermal instability of the X-ray tube. The X-ray generator manufacturer recommends half an hour to start a measurement after the kilo-voltage and current were established. Not all the measurements followed this recommendation.

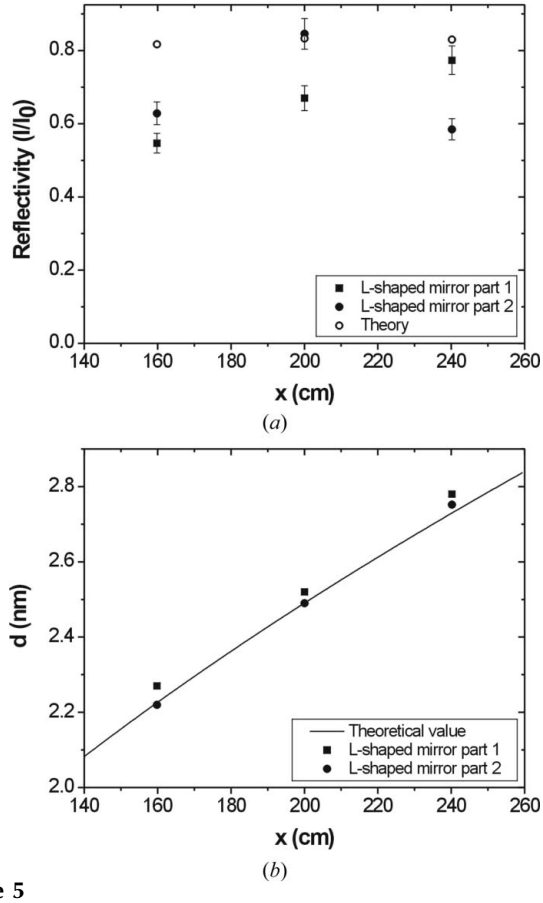

Figure 5
(*a*) Reflectivity values measured at three different points (A, B and C in Fig. 4) on both surfaces of the L-shaped laterally graded multilayer mirror. The theoretical reflectivity for the three different points is shown by opened circles. (*b*) Lattice parameter, *d*, acquired from the reflectivity measurements in the same three points (A, B and C in Fig. 4). The solid line shows the theoretical values of *d*.

We also checked the reflectivity of flat samples (sent by INCOATEC for conformance tests) which were coated just before and immediately after the mirror coating, with the same parameters as the L-shape mirror. The reflectivity of these flat samples agreed very well with the theoretical values. We should emphasize here that these measurements were taken at a lower energy (Cu $K\alpha_1$, 8.048 keV) that absorbs more than the working energy at 9.1 keV. So, the reflectivity at the working energy is expected to be 3–5% higher.

In Fig. 5(*b*) the extracted *d* values at the three different points for each surface are presented. They agree very well, within the error bars, with the theoretical values. The main contribution to the error bars is the uncertainty in the zero angle determination in the θ–θ diffractometer as discussed earlier. We also extracted the *d* values of the flat conformance samples and found that they agreed with the theoretical values with deviations of less than 1%. It is worth noting that a poor match between the theoretical and measured reflectivities does not mean that one cannot achieve a good match between the theoretical and measured *d* values. Even by not waiting for the X-ray generator stabilization the angles could be calibrated with reasonable accuracy.

5. Synchrotron X-ray tests

The use of the L-shaped laterally graded multilayer mirror as a synchrotron beamline component was tested at the NSLS-II R&D beamline at NSLS (X16A). The ideal experiment would have been to use the L-shaped laterally graded multilayer mirror as a collimating optic, for which a divergence source of 5 µm × 5 µm with a divergence of 5 mrad would be needed and can be generated in principle using the Ir $L\alpha_1$ fluorescent emission at 9.175 keV. Alternatively, one can also test the L-shaped laterally graded multilayer mirror reversely as a focusing optic. The results of this reverse test are reported here.

The experiment set-up is schematically shown in Fig. 6. The X16A flat bendable mirror was adjusted to have as much as possible a vertical collimated beam [$\sim$430 (V) µrad × 40 (H) µrad for a 1.2 (V) mm × 2.3 (H) mm beam]. The beamline Si 111 double-crystal monochromator (DCM) was set at an energy of 9.1 keV. This was calibrated, prior to this experiment, by a high-resolution monochromator, that has been tested at X16A at the exact back-diffraction condition for the Si 800 diffraction at 9.1 keV (Keister *et al.*, 2011). The L-shaped mirror was mounted 45° sagittally (inset in Fig. 6) in a He box, which was used to avoid radiation damage to the multilayers. The box was fixed in a $\theta/\chi/\varphi/x/z$ goniometer for the mirror alignment with the incoming beam. The 45° sagittal inclination allows the diffracted beam to remain in the vertical plane to simplify the alignment. After the mirror, three slightly different set-ups were used to exploit three different measurements: (i) *x*/*y* slits and a PIN diode detector to measure the reflectivity of both surfaces simultaneously; (ii) *x*/*y* slits and a PIN diode detector to measure the focus size (200 mm from the mirror) through knife-edge measurements; images of the focus were also taken at several distances from

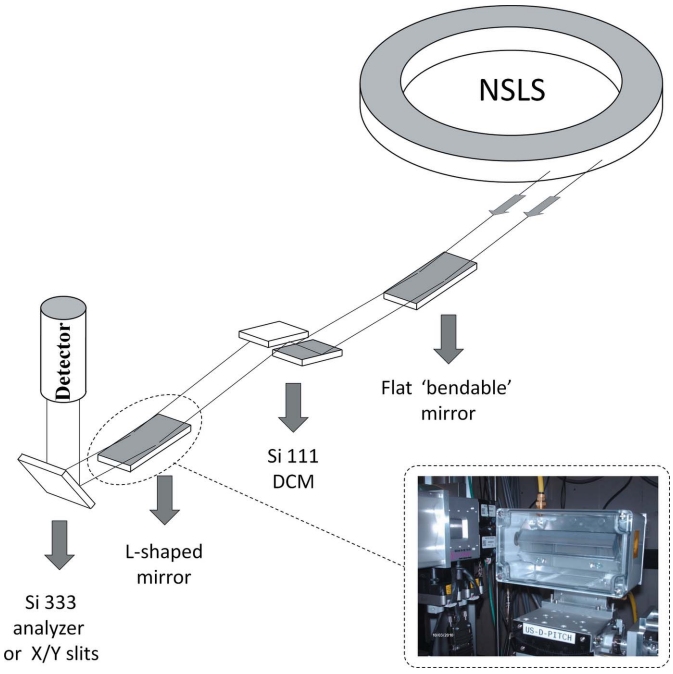

Figure 6
Experimental set-up at NSLS-II R&D beamline at NSLS (X16A) for the L-shaped laterally graded multilayer mirror tests. The flat bendable beamline mirror was bent in such a way as to take as much as possible a collimated beam. The double-crystal monochromator (DCM) was set at 9.1 keV, the working energy of the mirror. The L-shaped mirror was mounted sagittally at 45°. The mirror was set in a He-filled box (see the inset). To measure the focus size a set of slits was mounted at the mirror focal plane for knife-edge measurements. For reflectivity measurements a detector was mounted after the slits with the slits fully open. For divergence measurements a Si 333 crystal was mounted after the slits. By taking the rocking curve of this crystal with and without the mirror we could estimate the beam divergence.

the mirror (150–250 mm in steps of 3 mm each); (iii) *x*/*y* slits, Si 333 analyzer crystal and a scintillation detector to measure the divergence with and without the mirror.

In Fig. 7(*a*) a photograph of the experimental set-up for the reflectivity measurements is shown. The maximized reflectivity acquired from the diffraction of both surfaces, simultaneously, was found to be 52% (Fig. 7*b*). This is an excellent result, considering that in the specifications we expect to have 70% of reflectivity for each surface, *i.e.* 49% for both surfaces. Also, the FWHM of the curve is consistent with the theoretical value (∼415 µrad) which is close to the collimation of the incident beam. From the reflectivity curve shown in the inset some convoluted Pendellösung effects are clearly noticeable. These measurements were taken with the beam covering a mirror length of ∼40 mm. So, if Pendellösung fringes are still present, the stress in the multilayer film should be very low.

In Fig. 8(*a*) the focus size measurements taken with the film are shown. The same focus is shown as a three-dimensional image in Fig. 8(*b*). There is noticeable saturation in the image, even with the exposure time being around 1 s. We did not use attenuators to avoid spreading the focus owing to scattering in the attenuation foils. The dashed lines shown in Fig. 8(*a*) indicate the focus size extracted from the knife-edge

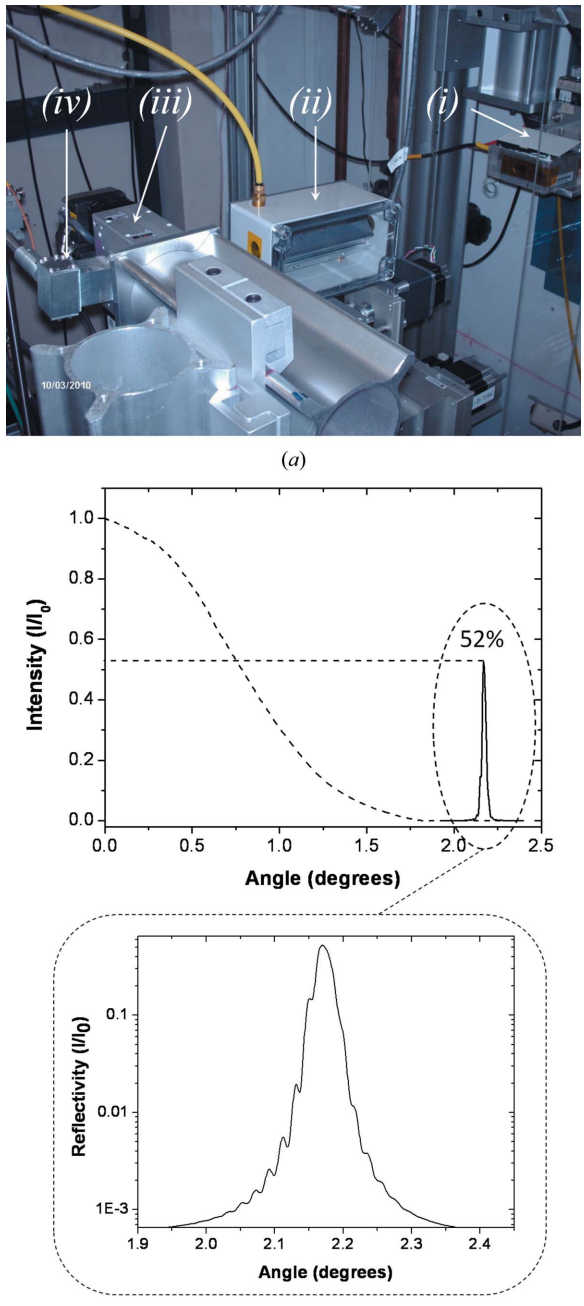

Figure 7
(*a*) Photograph of the experiment set-up for the reflectivity measurement taken in the hutch of R&D NSLS-II beamline at NSLS (X16A). (i) Ionization chamber, (ii) L-shaped mirror, (iii) *x*/*y* slits, (iv) PIN diode detector. (*b*) Reflectivity curve taken from both surfaces simultaneously. The inset shows details of the reflectivity curve showing convoluted Pendellösung effects from both surfaces.

measurements (scanning the vertical and horizontal slits). The derivative from the knife-edge data is shown in Figs. 8(*c*)–8(*f*). A focus size of ∼25 (V) µm × 32 (H) µm was found. In contrast, if the incoming beam had dimensions of 1.5 (V) mm × 1.5 (H) mm and a divergence of 57 µrad × 57 µrad, the theoretical spot size should be 5 µm × 5 µm according to our earlier ray-tracing studies (Honnicke *et al.*, 2010). However, our incoming beam did not have these properties. To under-

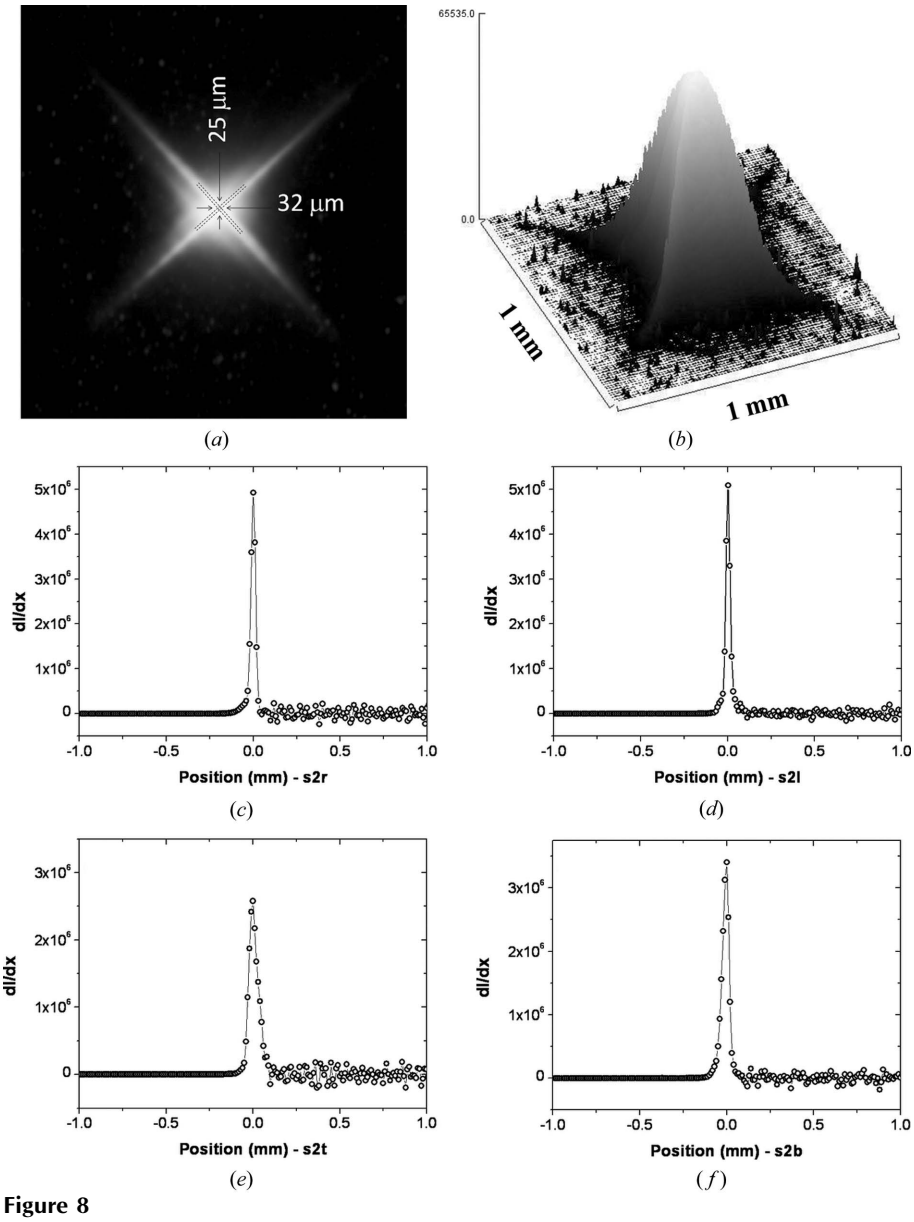

Figure 8
Focus size measurements (*a*) taken with the film at the focus position. The focus position was determined with an accuracy of 1 mm. (*b*) Three-dimensional image of the focus in (*a*). There is a noticeable saturation in the image even for a low exposure time (1 s). Attenuators were not used to avoid focus spreading owing to the scattering in the attenuator foils. (*c*) Derivative of the knife-edge measurements taken by scanning the right-hand slit (horizontal divergence). (*d*) Derivative of the knife-edge measurements taken by scanning the left-hand slit (horizontal divergence). (*e*) Derivative of the knife-edge measurements taken by scanning the top slit (vertical divergence). (*f*) Derivative of the knife-edge measurements taken by scanning the bottom slit (vertical divergence). By taking the average values between the right-hand and left-hand and bottom and top we found a focus size of 25 (V) μm × 32 (H) μm.

stand the measured results, we carried out further ray-tracing simulations taking into account the actual incident beam conditions to check whether the measured focus size was within the theoretically expected value.

Fig. 9(*a*) shows a photograph of the vertical divergence measurement. The vertical divergence was measured by rocking the Si 333 analyzer crystal for the incoming beam with and without the L-shaped mirror (Fig. 9*b*). Without the mirror the measured vertical divergence was ∼430 μrad. With the mirror the measured vertical divergence of the focused beam was 4.9 mrad. Both values were obtained with an incoming beam of 1.2 (V) mm × 2.3 (H) mm. Si 333 was chosen as an analyzer crystal because at 9.1 keV it shows a narrower intrinsic rocking curve width (∼10 μrad). However, the measured rocking curve will be broader owing to dispersion with the Si 111 DCM. The theoretical Si 333 rocking curve, taking into account the bandwidth contribution, is shown in Fig. 9(*c*). Without the mirror the horizontal divergence was defined by the slits to be 40 μrad. With the mirror, the horizontal divergence (6.8 mrad) was found based on the focus sizes at different distances from the mirror.

With the measurements completed, we tried to estimate the expected focal size of the mirror with the incoming beam properties of X16A. Two approaches were employed: (i) use our in-house ray-tracing code (Honnicke *et al.*, 2010) to estimate the size and divergence of the incoming beam for a measured focal size of 25 (V) μm × 32 (H) μm and divergence of 4.9 (V) mrad × 6.8 (H) mrad; (ii) perform the same simulation using *SHADOW* (Lai & Cerrina, 1986), but for a non-graded L-shaped multilayer mirror, since *SHADOW* cannot handle laterally graded multilayer mirrors.

The results of the first approach are shown in Fig. 10 and in Table 1. Two sets of results are shown: the first one is the expected incident beam size for a focal size of 25 (V) μm × 25 (H) μm and divergence of 4.9 (V) mrad × 4.9 (H) mrad; the second one is the expected beam size for a focal size of 32 (V) μm × 32 (H) μm and divergence of 6.8 (V) mrad × 6.8 (H) mrad. From these results and Table 1, one can see that the incident beam size should be ∼1.95 (V) mm × 2.5 (H) mm with a divergence of ∼143 (V) μrad × 92 (H) μrad.

A similar simulation was carried out using *SHADOW* for a non-graded multilayer mirror. The expected incident beam size for a focal size of 25 (V) μm × 32 (H) μm and divergence of ∼4.9 (V) mrad × 6.8 (H) mrad is shown in Fig. 11(*a*). The expected incident beam divergence is shown in Fig. 11(*b*). From these results one can see that the incident beam size should be ∼1.4 (V) mm × 1.6 (H) mm with a divergence of ∼130 (V) μrad × 100 (H) μrad. Analyzing these two simula-

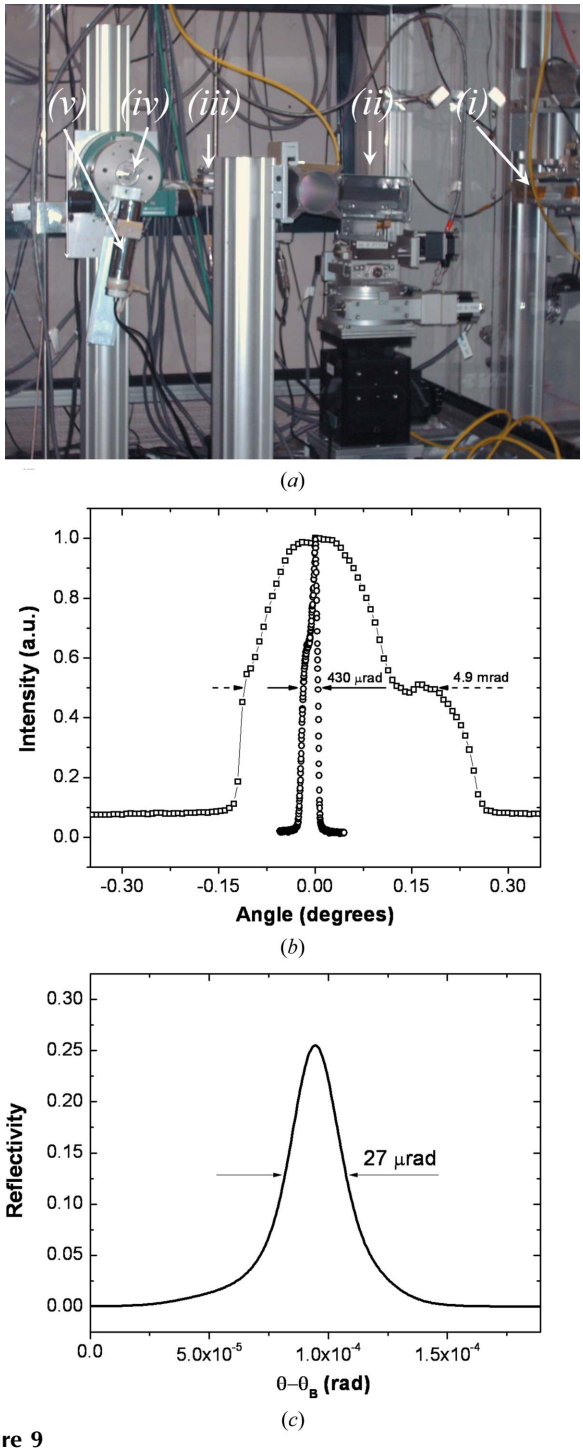

Figure 9
(*a*) Photograph of the experiment set-up for the divergence measurement taken in the hutch of the R&D NSLS-II beamline at NSLS (X16A). (i) Ionization chamber, (ii) L-shaped mirror, (iii) *x*/*y* slits, (iv) Si 333, (v) scintillation detector. (*b*) Divergence measurements without the mirror (opened circles) and with the mirror (opened squares). (*c*) Calculated bandwidth contribution for the Si 333 measured rocking curves where θ is the diffraction angle (refraction corrected) and θ_B is the Bragg angle.

tions one can see that the main discrepancy is the measured vertical divergence of the incoming X-ray beam. The other values (vertical and horizontal incident beam sizes and horizontal divergence) are in agreement with the measured data.

Table 1
Divergence and spot size for different source sizes for the parabolic L-shaped laterally graded multilayer mirror working as a collimating optics.

Angular acceptance (5 mrad × 5 mrad), slope error (10 μrad) and roughness (0.2 nm) are fixed. Such results were obtained from our previous work (Honnicke *et al.*, 2010) and from the ray-tracing simulations shown in Fig. 10.

Source size (μm)	Spot size (mm)	Divergence (μrad)
5 × 5	1.371 × 1.371	57
25 × 25	1.946 × 1.946	92
32 × 32	2.454 × 2.454	143

The reason for the discrepancy in the measured vertical divergence of the incoming X-ray beam could be some chromatic contribution owing to the beamline mirror curvature. This could be detected by the Si 333 analyzer crystal, which shows an energy resolution ($\Delta\lambda/\lambda$) of $\sim 10^{-5}$ but not detected with the L-shaped laterally graded multilayer mirror ($\Delta\lambda/\lambda \simeq 10^{-3}$). We can check on this by looking to the rocking curves of the Si 333 analyzer crystal and the L-shaped laterally graded multilayer mirror measured with the incoming X-ray beam at X16A. The measured FWHM for Si 333 is ∼430 μrad while for the L-shaped laterally graded multilayer mirror it is ∼415 μrad. The last value is the theoretical value for a plane and monochromatic X-ray beam, *i.e.* it is not affected by the divergence and chromaticity.

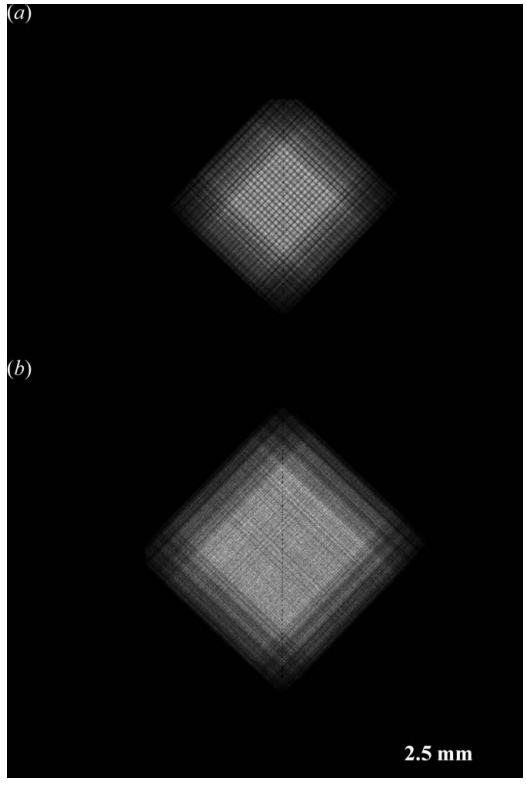

Figure 10
Simulated spot sizes for the parabolic L-shaped laterally graded multilayer mirror. The images were taken at 10 m from the mirror. The pixel size is approximately 2 μm × 2 μm. The acceptance is 5 mrad × 5 mrad, the source sizes are (*a*) 25 μm × 25 μm and (*b*) 32 μm × 32 μm. Slope error = 10 μrad, σ = 0.2 nm, $\Delta d/d = 7 \times 10^{-4}$.

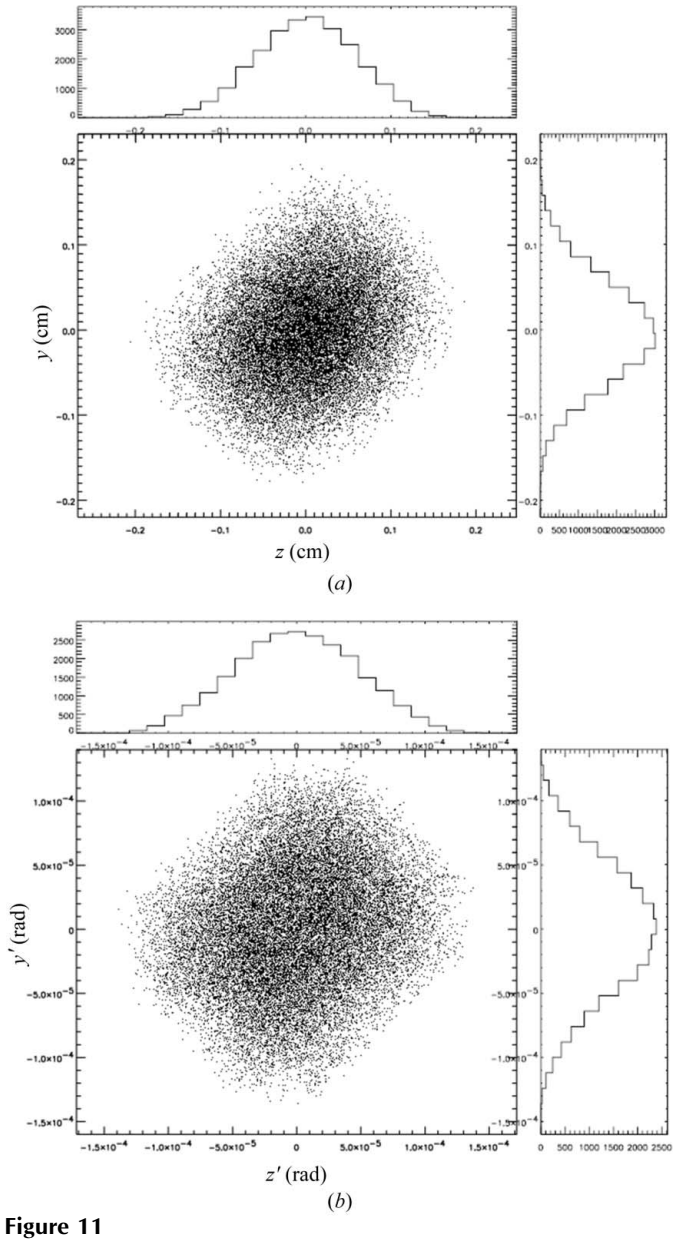

Figure 11
The same simulation shown in Fig. 10 but using *SHADOW* for a non-laterally graded L-shaped multilayer mirror. (*a*) Spot size; (*b*) divergence. The results are consistent with the results shown in Fig. 10.

6. Conclusion

An L-shaped laterally graded multilayer mirror (nested or Montel Kirkpatrick–Baez mirrors) was successfully tested as a synchrotron beamline optical element. The mirror characterization (reflectivity and metrology) showed that it was within the specifications. The synchrotron tests showed that the mirror can also be used for synchrotron applications. The measured reflectivity (52%, measured as the contribution from both reflecting surfaces), divergence [4.9 (V) mrad × 6.8 (H) mrad] and spot size [25 (V) μm × 32 (H) μm] are compatible with the incident-beam properties at NSLS-II R&D beamline at NSLS (X16A), and show that the L-shaped laterally graded multilayer mirror will be a workable high-efficiency optical device in the analyzer system of the future ultra-high-resolution inelastic X-ray scattering (IXS) spectrometer at NSLS-II. It is worth noting that in the real configuration the effects of multilayer inhomogeneity and slope errors can be different. So, a deeper experimental study should be carried out in the real configuration to prove that this is not the case.

This work was supported by the US Department of Energy, Office of Science, Office of Basic Energy Sciences, under contract No. DE-AC-02-98CH10886.

References

Authier, A. (2001). *Dynamical Theory of X-ray Diffraction.* Oxford University Press.
Cai, Y. Q., Coburn, S., Cunsolo, A., Honnicke, M. G., Huang, X. R., Keister, J. W., Kodituwakku, C. N., Chubar, O. & Ravindranath, V. (2009). *Conceptual Design Report for the Inelastic X-ray Scattering Beamline at NSLS-II.* Unpublished.
Champeaux, J.-Ph., Troussel, Ph., Villier, B., Vidal, V., Khachroum, T., Vidal, B. & Krumrey, M. (2007). *Nucl. Instrum. Methods Phys. Res. A*, **581**, 687–694.
DuMond, J. & Youtz, J. P. (1940). *J. Appl. Phys.* **11**, 357–365.
Hertlein, F., Oehr, A., Hoffmann, C., Michaelsen, C. & Wiesmann, J. (2005). *Part. Part. Syst. Charact.* **22**, 378–383.
Honnicke, M. G. & Cusatis, C. (2009). *J. Appl. Cryst.* **42**, 999–1003.
Honnicke, M. G., Huang, X., Keister, J. W., Kodituwakku, C. N. & Cai, Y. Q. (2010). *J. Synchrotron Rad.* **17**, 352–359.
Ice, G. E., Pang, J. W. L., Tulk, C., Molaison, J., Choi, J.-Y., Vaughn, C., Lytle, L., Takacs, P. Z., Andersen, K. H., Bigault, T. & Khounsary, A. (2009). *J. Appl. Cryst.* **42**, 1004–1008.
Keister, J. W., Stetsko, Y., Cunsolo, A., Honnicke, M. G., Huang, X. R., Kodituwakku, C. N., Coburn, S. & Cai, Y. Q. (2011). In preparation.
Kirkpatrick, P. & Baez, A. V. (1948). *J. Opt. Soc. Am.* **38**, 766–774.
Lai, B. & Cerrina, F. (1986). *Nucl. Instrum. Methods Phys. Res. A*, **246**, 337–341.
Lienert, U., Poulsen, H. F., Honkimäki, V., Schulze, C. & Hignette, O. (1999). *J. Synchrotron Rad.* **6**, 979–984.
Liu, W., Ice, G. E., Assoufid, L., Liu, C., Shi, B., Khachatryan, R., Qian, J., Zschack, P., Tischler, J. Z. & Choi, J.-Y. (2011). *J. Synchrotron Rad.* **18**, 575–579.
Schuster, M. & Gobel, H. (1995). *J. Phys. D*, **28**, A270–A275.
Shvyd'ko, Yu. V., Lerche, M., Kuetgens, U., Ruter, H. D., Alatas, A. & Zhao, J. (2006). *Phys. Rev. Lett.* **97**, 235502.
Shymanovich, U., Nicoul, M., Sokolowski-Tinten, K., Tarasevitch, A., Michaelsen, C. & Von der Linde, D. (2008). *Appl. Phys. B*, **92**, 493–499.
Vinogradov, A. V. & Zeldovich, B. Y. (1977). *Appl. Opt.* **16**, 89–93.